Simple framework for understanding the universality of the maximum drag reduction asymptote in turbulent flow of polymer solutions

Chang-Feng Li,[1,2] Radhakrishna Sureshkumar,[3] and Bamin Khomami[2,*]

[1]*School of Energy and Power Engineering, Jiangsu University, Zhenjiang, Jiangsu 212013, People's Republic of China*

[2]*Materials Research and Innovation Laboratory, Department of Chemical and Biomolecular Engineering, University of Tennessee, Knoxville, Tennessee 37996, USA*

[3]*Department of Biomedical and Chemical Engineering, Syracuse University, Syracuse, New York 13244, USA*

(Received 5 January 2015; revised manuscript received 16 April 2015; published 21 October 2015)

Self-consistent direct numerical simulations of turbulent channel flows of dilute polymer solutions exhibiting friction drag reduction (DR) show that an effective Deborah number defined as the ratio of polymer relaxation time to the time scale of fluctuations in the vorticity in the mean flow direction remains $O(1)$ from the onset of DR to the maximum drag reduction (MDR) asymptote. However, the ratio of the convective time scale associated with streamwise vorticity fluctuations to the vortex rotation time decreases with increasing DR, and the maximum drag reduction asymptote is achieved when these two time scales become nearly equal. Based on these observations, a simple framework is proposed that adequately describes the influence of polymer additives on the extent of DR from the onset of DR to MDR as well as the universality of the MDR in wall-bounded turbulent flows with polymer additives.

DOI: 10.1103/PhysRevE.92.043014 PACS number(s): 47.27.ek, 83.60.Yz, 47.27.nd, 47.57.Ng

I. INTRODUCTION

It is well known that the addition of a small amount of soluble high–molecular-weight polymers to wall-bounded turbulent flows can lead to dramatic friction drag reduction (DR). Polymer concentrations of $O(100)$ ppm are sufficient to reduce the drag by up to 80% [1–5]. This phenomenon has enormous practical applications, including reducing the cost of transportation of crude oil over long distances. Two salient features of this phenomenon are the existence of a threshold for the onset of drag reduction and an upper bound referred to as the maximum drag reduction (MDR) asymptote, originally proposed by Virk [6] based on his extensive analysis of experiments conducted using homogeneous polymer solutions that varied in chemical detail, concentration, and molecular weight. Since the mid-1990s, direct numerical simulations (DNSs) of turbulent flows (see, for example, Refs. [7–13]), in which one self-consistently solves the equations of conservation of mass and momentum with an evolution equation for the polymeric stresses such as the finitely extensible nonlinear elastic Peterlin (FENE-P) model, have been successfully performed.

DNS results have demonstrated that polymer-induced DR arises as a consequence of a self-sustaining process that relies on significant polymer chain extension in the near-wall region and a commensurate extraction of energy from the fluctuating motions, and the stabilization of near-wall streamwise vortices [4,5,7,10,11,14–17]. The polymer extensional viscosity has a remarkable effect on the aforementioned self-sustaining process and the extent of DR [11,14–17]. In parallel to DNSs, DR has also been investigated from the point of view of coherent structure (CS) dynamics [18–23]. These studies show that the action of quasistreamwise vortices leads to substantial chain elongation and commensurate polymeric forces and torques that inhibit CS dynamics responsible for the production of turbulent shear (Reynolds) stress. The proposed suppression of streak instability and the commensurate self-sustaining mechanism [18,19], the effect of biaxial extensional flow [21], and the inhibition of autogeneration of new vortices [23] are among the principal findings of DNS and CS dynamics studies. In particular, it has been shown that enhanced chain extensibility or extensional viscosity results in enhanced DR via modification of near-wall coherent structures; i.e., energetic streamwise vortices exhibit a significant reduction in number and become highly elongated. Moreover, simulations have shown the existence of an onset threshold for DR, at an $O(1)$ Deborah number defined as the ratio of the polymer relaxation time to the time scale of fluctuations in the vorticity in the mean flow direction.

While these studies have clearly indicated that the interaction of polymer and vortex time scales play a central role in determining the extent of DR, a clear interpretation and a criterion for the existence of MDR in this context are lacking. In this study, we report specific criteria for interaction of polymer and vortex time scales for the onset of DR and the MDR asymptote.

II. NUMERICAL METHODS

For the channel Poiseuille flow considered in this study, the x axis represents the mean flow direction, i.e., the direction of the constant, externally imposed pressure gradient, and the y and z axes are the wall-normal and spanwise directions respectively. The nondimensional governing equations for unsteady, incompressible, viscoelastic flow with the FENE-P constitutive equation are as follows:

$$\nabla \boldsymbol{u} = 0, \tag{1}$$

$$\boldsymbol{u}_t + \boldsymbol{u}\,\nabla \boldsymbol{u} = -\nabla p + \frac{\beta}{\mathrm{Re}_\tau}\nabla^2 \boldsymbol{u} + \frac{1-\beta}{\mathrm{Re}_\tau}\nabla \tau, \tag{2}$$

$$c_t + \boldsymbol{u}\nabla c = c\nabla \boldsymbol{u} + (\nabla \boldsymbol{u})^T\, c - \tau, \tag{3}$$

*Corresponding author: bkhomami@utk.edu

where $\boldsymbol{u}$ is the velocity, p is the pressure, and the polymer stress $\boldsymbol{\tau} = \{\boldsymbol{c}/[1 - \mathrm{Tr}(\boldsymbol{c})/L^2] - \boldsymbol{I}\}/\mathrm{We}_\tau$. The friction velocity U_τ and the channel half height h are used as the velocity and length scales, respectively. The friction velocity is defined as $U_\tau = (\tau_w/\rho)^{1/2}$, where τ_w represents the shear stress at the wall and ρ is the density of the polymer solution. The frictional Reynolds number is defined as $\mathrm{Re}_\tau = U_\tau h/\nu_0$, where ν_0 is the zero shear-rate kinematic viscosity. The parameter β is the ratio of the solvent viscosity (μ_s) to the total solution zero-shear-rate viscosity (μ_0). The polymer stress $\boldsymbol{\tau}$ is obtained by solving an evolution equation for the conformation tensor $\mathbf{c}\langle\mathbf{qq}\rangle$, which represents the average second moment of the polymer chain end-to-end distance vector ($\boldsymbol{q}$). Note that $|\boldsymbol{q}| < L$ since L represents the maximum length of the macromolecule.$\boldsymbol{I}$ is the unit tensor, and $\mathrm{We}_\tau = \lambda {U_\tau}^2/\nu_0$ is the friction Weissenberg number, a dimensionless relaxation time defined as the product of the polymer relaxation time (λ) and a characteristic shear rate based on the friction velocity. As in earlier DNSs of turbulent viscoelastic flows, a small artificial diffusive term $D\nabla^2\boldsymbol{c}$ must be added to the right-hand side of Eq. (3) to enhance numerical stability. Specifically, we have used a very small D, namely $O(0.01)$, resulting in a numerical Schmidt number $\mathrm{Sc}^+ = 1/(\mathrm{Re}_{\tau 0} D)$ of $O(0.1)$, for which the elastically modified turbulent flow structures are D independent. Note that the original constitutive equation without the diffusive term is applied at the walls; thus, no boundary conditions are externally imposed for $\boldsymbol{c}$ at the wall.

The fully spectral numerical method used for solving the governing equations, the rheological parameter sets, turbulence statistics, and the extent of DR are described in detail in our earlier publications [11–13]. It should be noted that the present simulation results are obtained from streamwise computational domains of approximately 5000 and 10 000 wall units. Although these domains are two or four times longer than those commonly used for Newtonian flow simulations, they are essential for obtaining accurate vorticity correlations [11]. The spatial discretization, i.e., mesh resolution, is $\Delta x^+ \approx 20$ in the low-drag-reduction (LDR, 0 < DR < 30%) and high-drag-reduction (HDR, 30% < DR < 60%) regimes, while $\Delta x^+ \approx 40$ is used at MDR; $\Delta z^+ \approx 10$ and $\Delta y^+ \approx 0.06$ near the wall (the Chebyshev node spacing is nonuniform in the y direction, i.e., it is much more refined in the wall region) is used to ensure sufficient resolution [11–13].

The numerical value of We_τ for onset of DR depends on the ratio of solvent to total viscosity β as well as the maximum chain extensibility L, in units of $(kT/H)^{1/2}$ (H is defined as the spring constant of the FENE-P bead-spring model, and kT is the energy of thermal fluctuations), i.e., $(1 - \beta)L^2\ \mathrm{We}_\tau$ could be thought of as a measure of the cumulative elastic effect of the polymer additive [14–17]. Similarly, more recent DNS studies [10,11,16] have shown that as $L^2\mathrm{We}_\tau$ approaches a large enough value, DR plateaus at around 70%.

The value of β is inversely related to the polymer concentration. Since most prior DNS studies of polymer-induced turbulent DR have been performed for bulk flows with a mean Reynolds number less than 8900, they have used lower β values than those in the experiments to amplify elastic effects. In fact, β values as low as 0.4 have been used [10] in order to reach the HDR regime. However, such β values lead to significant shear thinning of the viscosity, and special care should be taken to define the DR accurately. Hence, we have chosen $\beta = 0.9$ to perform our simulations as it has been shown that with this value one can capture elastic effects with negligible influence of shear-thinning viscosity (i.e., on the order of a few percent) [11–13]. The high level of turbulent fluctuation with respect to the mean value in the MDR regime has been clearly shown in [11]. Specifically, the variations in the xz plane averaged data are relatively minor at LDR. Hence, time averaging over 10–15 computational units (h/U_τ) is sufficient to obtain good statistics, while in the HDR and MDR regimes significant variations are observed. Since the degree of intermittency rapidly increases as one moves from the LDR to the HDR and MDR regimes, time averaging over $30 - 50\, h/U_\tau$ is needed to obtain good statistics.

III. RESULTS AND DISCUSSION

Figure 1 shows a typical mean streamwise velocity profile as a function of the distance from the wall for the simulations conducted at $\mathrm{Re}_{\tau o} = 395$. Clearly, two DR regimes can be observed with low drag reduction and high drag reduction [10,24]. In the LDR regime, the logarithmic profile is shifted upwards parallel to that of the Newtonian flow, while in the HDR regime, the slope of the mean velocity is augmented gradually with the increasing DR levels. Finally, for the 74% DR case, Virk's MDR asymptote ($U^+ = 11.7 \ln y^+ - 17$) is observed. The turbulence statistics in the LDR and HDR regimes are distinctly different. At LDR, the statistics are similar to those for Newtonian flows; however, at HDR significant reduction in normal and spanwise velocity fluctuations and Reynolds stress is observed [10,11,24].

Typical vorticity fluctuations at various DR levels up to MDR have been shown in [11]. The intensity of the streamwise vorticity fluctuations monotonically decreases with increasing DR. The average size of the vortices also increases and the location of the center of the energetic vortices shifts to the center of the channel. The circles shown in Fig. 2 schematically represent the average size and position of the streamwise vortices at different extents of DR. The locations of the maximum and minimum correspond to the average edge and center locations of the streamwise vortices (eddies) in the

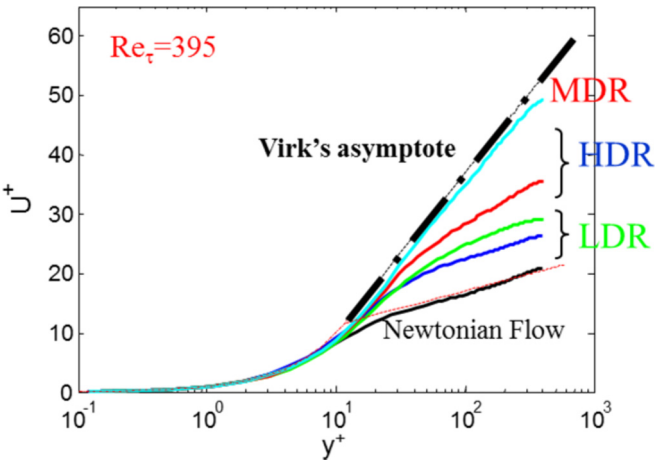

FIG. 1. (Color online) Mean streamwise velocity profiles as a function of distance from the wall.

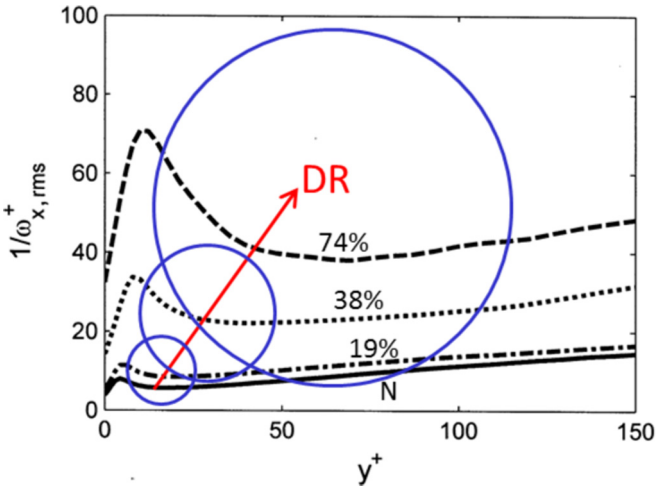

FIG. 2. (Color online) The axial vortex rotation time scale $1/\omega^+_{x,\mathrm{rms}}$ as a function of the distance from the wall. The circles sketch the sizes and positions of energetic vortices.

wall region, respectively [25]. The interval between these two locations is roughly the average radius of streamwise vortices. It can be seen that at MDR the average size of the streamwise energetic vortices is larger than 100 wall units, i.e., on the order of the flow channel outer scale.

It is well known that the streamwise vortices play an important role in mediating the mass and momentum transfer between the near-wall region and the turbulent core by ejecting low-speed fluid from the near-wall region to the core (ejection or upwash). In addition, they bring high-speed fluid from the core towards the wall (sweep or downwash). The time scale associated with such events can be estimated as the inverse of the root mean square vorticity fluctuations $\omega_{x,\mathrm{rms}}$ and the product $\lambda\omega_{x,\mathrm{rms}}$. Lumley [1,2] has conclusively demonstrated the drag reducing effect of polymer additives as follows. Macromolecules are streched in the flow outside the viscous sublayer due to the fluctuating strain rate. In a flow field with a characteristic deformation (shear) rate, and a corresponding fluctuating strain rate of U_τ^2/ν, the degree of polymer stretch is directly related to the friction Weissenberg number $\mathrm{We}_\tau = \lambda U_t^2/\nu$. If $\mathrm{We}_\tau \ll 1$, then macromolecules have sufficient time to relax to equilibrium; hence, their effect on the flow is minimal. However, when We_τ reaches an $O(1)$ value, polymers can be significantly stretched by the flow and the extent of the macromolecular stretch is intimately related to the flow kinematics. Thus, $\lambda\omega_{x,\mathrm{rms}}$ on average represents the number of stretching and relaxation cycles the polymer undergoes within a single vortex rotation. As shown in Fig. 2, $1/\omega^+_{x,\mathrm{rms}}$ (scaled by the time scale of viscous diffusion ν/U_τ^2) increases with increasing DR. It can also be seen that for Newtonian flows in the viscous sublayer and the buffer layer this time scale is in the range of five to ten times the viscous diffusion time scale. If drag reduction is manifested when these time scales at small y^+ become equivalent (i.e., the dimensionless time scales for upwash and downwash become similar to We_τ), then one would expect that the onset of DR occurs in the range $5 \leqslant \mathrm{We}_\tau < 10$. Indeed, this is consistent with the findings for the onset of drag reduction at $\mathrm{We}_\tau = 6.25$ (i.e., Deborah number $\mathrm{De} = \lambda\omega_{x,\mathrm{rms}} = \mathrm{We}_\tau\omega^+_{x,\mathrm{rms}} \sim O(1)$ [1,2,26]).

TABLE I. The comparison of $\mathrm{We}_\tau^{\mathrm{eff}}$ and $1/\omega^+_{x,\mathrm{rms}}$ in the near-wall region.

We_τ	L^2	DR	$\mathrm{Tr}(c)/L^2$	$\mathrm{We}_\tau^{\mathrm{eff}}$	$1/\omega^+_{x,\mathrm{rms}}$
0					~5–10
25	900	19%	~0.35	~15	~10–16
100	900	38%	~0.78	~22	~20–32
100	3600	54%	~0.62	~38	~30–45
100	14400	61%	~ 0.42	~58	~38–68
200	14400	74%	~ 0.77	~66	~42–72

This analysis clearly suggests that the near-wall vortex time scale plays a significant role in determining the onset of DR. In fact, in addition to the onset of DR we have observed that this time scale plays a significant role in all DR regimes. Polymers extract energy from the flow as they are pulled around the near-wall vortices, and release energy back to the flow in the high-speed streaks [17]. Hence, the degree to which the polymer chains have been extended should be considered in analyzing the results. Thus an effective Weissenberg number $\mathrm{We}_\tau^{\mathrm{eff}} = \mathrm{We}_\tau[1 - \mathrm{Tr}(\boldsymbol{c})/L^2]$ is a more appropriate measure of the polymer time scale for understanding the interplay between the polymer chain and the flow dynamics. It should be noted that $[1 - \mathrm{Tr}(c)/L^2]$ appears in the expression for the polymeric stress tensor. The values of $\mathrm{We}_\tau^{\mathrm{eff}}$ and $1/\omega^+_{x,\mathrm{rms}}$ n the near-wall region are listed in Table I.

Clearly, from the onset of DR up to the MDR asymptote, $\mathrm{We}_\tau^{\mathrm{eff}}$ is increased from 5–10 to about 60–70, while the product of $\mathrm{We}_\tau^{\mathrm{eff}}\omega^+_{x,\mathrm{rms}}$ remains $O(1)$ in the near-wall region. This suggests that as elastic forces are enhanced they lead to stabilization of near-wall axial vortices, resulting in much longer and more slowly rotating vortices. Furthermore, these findings underscore the fact that there exists an intricate balance between elastic forces and average rotation speed of the near-wall axial vortices that determines upwash and downwash events and consequently Reynolds stress production.

To shed light on the exact mechanism by which polymer-induced drag reduction occurs various time scales should be carefully examined. To this end, we have defined an effective Deborah number $\mathrm{De}^{\mathrm{eff}}$ that signifies the ratio of polymer to the near-wall region vortex time scale, i.e., $\mathrm{De}^{\mathrm{eff}} = \mathrm{We}_\tau^{\mathrm{eff}}\omega^+_{x,\mathrm{rms}}$. This time scale remains $O(1)$ from the onset of DR to MDR. Hence, the polymer releases sufficient energy to stabilize the vortices such that a self-sustaining mechanism of drag reduction is maintained. It should be noted that, in this self-sustaining mechanism, the vortex convection velocity is another important factor in determination of the average vortex dynamics. The vortex convection time can be estimated from the average vortex length divided by the vortex convection velocity. To this end we have examined the convection velocity of the streamwise vorticity perturbations based on a method proposed by Kim and Hussain [27]. Specifically, the space-time cross correlations are used to evaluate the convection velocity for the vorticity perturbations in the mean flow direction. At a given y-plane location, the space-time cross correlation for streamwise vorticity perturbations is

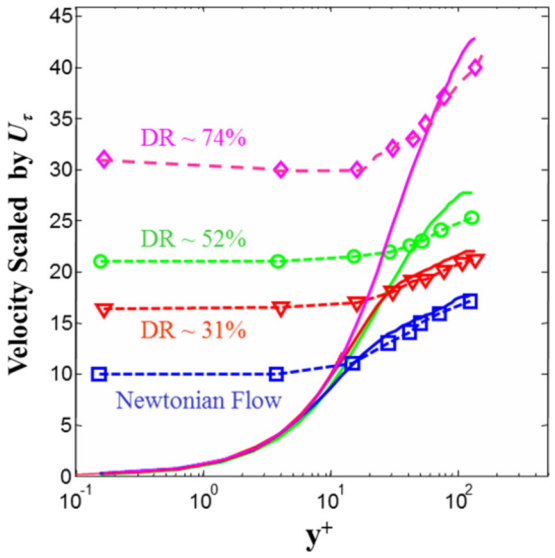

FIG. 3. (Color online) The convection velocities for the vorticity perturbations in the flow direction at different extents of DR.

given by

$$R_{\omega_x\omega_x}(\Delta x^+, y^+, \Delta t^+) = \frac{\overline{\omega_x(x^+, y^+, t^+)\omega_x(x^+ + \Delta x^+, y^+, t^+ + \Delta t^+)}}{\omega^+_{x,\,\mathrm{rms}}(y^+)\omega^+_{x,\,\mathrm{rms}}(y^+)}.$$

The signal convection velocity V_c is the velocity with which the main portion of the signal amplitude travels, and it can be measured by the peak location of space-time cross correlations for a given time interval Δt [27]. In turn, this velocity is scaled by the friction velocity U_τ, $V_c{}^+ = \Delta x^+_{\mathrm{peak}}/\Delta t^+$. Figure 3 shows the convection velocities for vorticity perturbations in the flow at different extents of DR. It is now widely accepted that for Newtonian flows the axial vorticity perturbations propagate at a constant speed of $\sim 10U_\tau$ at $y^+ < 10$. It can be seen that, with increasing DR, the same feature is more or less observed. That is the convection velocities are increased and the constant convection velocity regions are also thickened. The intersection points between the convection velocity curves and the mean velocity profiles can be roughly regarded as the center of energetic axial vortices. This implies that in drag-reduced flows the energetic axial vortices propagate at higher speeds and with significantly increased size. Specifically, at MDR the average axial energetic vortex moves at least three times faster than its Newtonian counterpart and it is also at least three times larger than the Newtonian vortex.

The aforementioned time scales, the vortex rotation time and axial vortex convective time as a function of DR, are shown in Fig. 4. Since the vortex length increase is larger than the vortex convection velocity increase, the approximate time scale for persistence of axial vorticity perturbation, dubbed the vortex lifetime, must increase with the extent of DR. The ratio of the average vortex convection time to the average vortex rotation time is also plotted in Fig. 4 (see the right vertical coordinate). It can be seen that although the average lifetime of axial vortices increases with increasing DR while their rotation speed decreases, the rate of decrease in the rotation speed exceeds the enhancement in lifetime of axial vortices as a

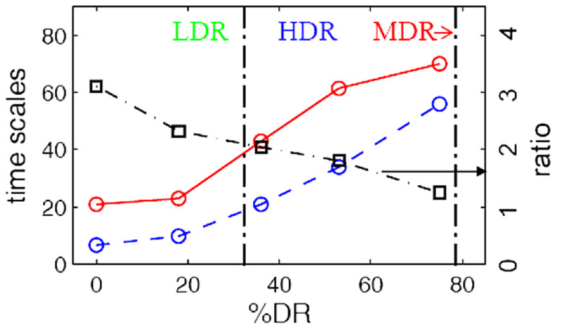

FIG. 4. (Color online) The average time scales and ratio of axial vortex convective time to vortex rotation time as a function of extent of DR. —⊙— axial vortex convection time; --⊙-- vortex rotation time; –·–□–·– the ratio.

function of DR. In fact, this ratio starts at ~ 3 for Newtonian flows and becomes close to 1 as MDR is approached. For Newtonian flows, this result is consistent with the fact that there are on average three ejection events during one burst [28].

If this ratio (average vortex convection time to the average vortex rotation time scale) is reduced below 1, then a full vortex rotation process cannot on average be completed within a vortex convective time, and the intricate balance between elastic forces and vortex rotation will cease to exist. Thus MDR is reached when the aforementioned ratio becomes nearly equal, i.e., the energy extraction and release cycle gets interrupted. In turn, the flow state becomes weakly turbulent (laminarlike). Eventually, the system transits back to active turbulence and the stochastic cycle repeats. This observation is in agreement with the experimental remark by Virk [3] that close to the MDR asymptote the flow appears laminar and shows very high intermittency [11]. This proposed frame work is also consistent with the universal nature of MDR as it is based on an intricate flow microstructure coupling that balances the vortex lifetime and the vortex rotation time scale. Hence, MDR is reached irrespective of the specifics of polymer species, molecular weight, or the polymer-solvent pair.

These results clearly highlight that MDR is basically a transition state between laminarlike and turbulent flow. This is in agreement with the theory proposed in [29–31] that a linear viscosity profile growing with the distance from the wall reduces the drag in turbulent flows by polymers, and the MDR profile is an edge solution of the Navier-Stokes equations beyond which no turbulent solution exists. To this end, we have computed the effective viscosities for representative LDR and HDR cases as well as at MDR [see Fig. 5(a)]. Clearly, the effective viscosities increase linearly from the wall to their respective peak positions. Also, the peak positions progressively move towards the center of the channel as DR is enhanced. Evidently, the vortex size and the peak positions are intimately related, i.e., the vortices are bounded by the peak position of the effective viscosity which corresponds to the average sizes and positions of the streamwise energetic vortices, respectively (see Fig. 2). At MDR, the effective viscosity increases linearly up to $y/h = 0.4$, indicating that the vortex size is approximately 150 wall units ($\mathrm{Re}_{\tau 0} = 395$). Clearly, the extent to which highly stretched polymers are ejected to the "bulk flow" is a sensitive function of the

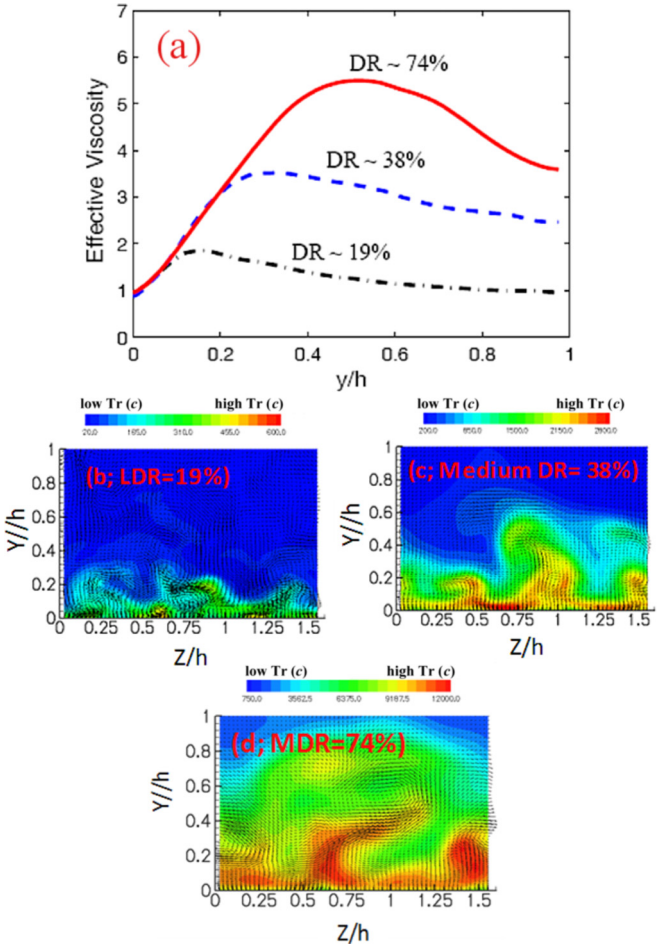

FIG. 5. (Color online) The effective viscosity (a) and instantaneous vectors and trace($\boldsymbol{c}$) distribution (b), (c), and (d) in the flow at different extents of DR.

aforementioned vortex sizes [see Figs. 5(b)—5(d)]. These results further underscore the fact that simulations and/or experiments at $\mathrm{Re}_{\tau 0} = 125$ and 180 are not at a high enough $\mathrm{Re}_{\tau 0}$ for a comprehensive study of polymer-induced drag reduction in the HDR and MDR regimes [11,31].

It is very gratifying that our simple framework based on the intricate coupling of the polymer and near-wall vortex dynamics is consistent with several recently proposed mechanisms of drag reduction by polymer additives. Examples include the following: (1) During vortex rotation (upwash and downwash events) elastic energy is stored in the stretched polymers in the very-near-wall region and in turn it is transported and released to the buffer and the logarithmic layers [17,32]. (2) The high intermittency of polymer work is consistent with the polymer effect being associated with intermittent near-wall structures such as quasistreamwise and hairpin vortices [15]. (3) The exact coherent state [14,15,20], where it has been shown that viscoelasticity has a weakening effect on the streamwise vortices, plus the fact that for sufficiently low values of the frictional Reynolds number ($\sim$45), the coherent structures could be entirely suppressed if the elastic effects are sufficiently large.

IV. CONCLUSION

In summary, the effect of polymer additives on vortex dynamics and the extent of DR has been elucidated via extensive analysis of high-fidelity DNSs of polymer-induced drag reduction in turbulent channel flows. Specifically, it has been shown that in the near-wall region, from the onset of DR to MDR, a modified effective Deborah number defined as the ratio of polymer relaxation time to the time scale of fluctuations in the vorticity in the mean flow direction remains $O(1)$.

Moreover, it has been demonstrated that the average axial energetic vortex convection time increases with increasing DR while its rotation speed decreases. However, the rate of decrease in the rotation speed exceeds the enhancement in lifetime of axial vortices as DR is increased. Hence, MDR is achieved when these two time scales become nearly equal. Overall, this simple framework can adequately describe the influence of polymer additives on the extent of DR from onset to MDR as well as the universality of the MDR in flow systems with polymer additives. We hope that this framework can also pave the way for modeling drag reduction in the HDR and MDR regimes.

ACKNOWLEDGMENTS

This work has been supported by DARPA (Grants No. MDA972-01-1-0007 and No. 29773A), NSFC (Grants No. 10672069 and No. 11072091), and Key Sci-Tech Project (Grant No. 210078) from Ministry of Education, China. This research was also supported in part by allocation of advanced computational resources on DARTER by the National Institute for Computational Sciences (NICS).

[1] J. L. Lumley, Annu. Rev. Fluid Mech. **1**, 367 (1969).
[2] J. L. Lumley, J. Polym. Sci. **7**, 263 (1973).
[3] P. S. Virk, AIChE J. **21**, 625 (1975).
[4] M. D. Graham, Rheol. Rev. **2**, 143 (2004).
[5] C. M. White and M. G. Mungal, Annu. Rev. Fluid Mech. **40**, 235 (2008).
[6] P. S. Virk, J. Fluid Mech. **45**, 417 (1971).
[7] R. Sureshkumar, A. N. Beris, and R. A. Handler, Phys. Fluids **9**, 743 (1997).
[8] E. De Angelis, C. M. Casciola, and R. Piva, Comput. Fluids **31**, 495 (2002).
[9] K. D. Housiadas and A. N. Beris, Phys. Fluids **15**, 2369 (2003).
[10] P. K. Ptasinski, B. J. Boersma, F. T. M. Nieuwstadt, M. A. Hulsen, B. H. A. A. Van den Brule, and J. C. R. Hunt, J. Fluid Mech. **490**, 251 (2003).
[11] C. F. Li, R. Sureshkumar, and B. Khomami, J. Non-Newtonian Fluid Mech. **140**, 23 (2006).
[12] N. Liu and B. Khomami, Phys. Rev. Lett. **111**, 114501 (2013).
[13] N. Liu and B. Khomami, J. Fluid Mech. **737**, R4 (2013).

[14] P. A. Stone, F. Waleffe, and M. D. Graham, Phys. Rev. Lett. **89**, 208301 (2002).
[15] P. A. Stone, A. Roy, R. G. Larson, F. Waleffe, and M. D. Graham, Phys. Fluids **16**, 3470 (2004).
[16] C. Dimitropoulos, Y. Dubief, E. S. G. Shaqfeh, and P. Moin, J. Fluid Mech. **566**, 153 (2006).
[17] Y. Dubief, C. M. White, V. E. Terrapon, E. S. G. Shaqfeh, P. Moin, and S. K. Lele, J. Fluid Mech. **514**, 271 (2004).
[18] W. Li and M. D. Graham, Phys Fluids **19**, 083101 (2007).
[19] A. Roy, A. Morozov, W. van Saarloos, and R. G. Larson, Phys. Rev. Lett. **97**, 234501 (2006).
[20] W. Li, L. Xi, and M. D. Graham, J. Fluid Mech. **565**, 353 (2006).
[21] V. E. Terrapon, Y. Dubief, P. Moin, E. S. G. Shaqfeh, and S. K. Lele, J. Fluid Mech. **504**, 61 (2004).
[22] K. Kim, C.F. Li, R. Sureshkumar, S. Balachandar, and R. J. Adrian, J. Fluid Mech. **584**, 281 (2007).
[23] K. Kim, R. J. Adrian, S. Balachandar, and R. Sureshkumar, Phys. Rev. Lett. **100**, 134504 (2008).
[24] M. D. Warholic, H. Massah, and T. J. Hanratty, Exp. Fluids **27**, 461 (1999).
[25] J. Kim, P. Moin and R. Moser, J. Fluid Mech. **177**, 133 (1987).
[26] F. A. Seyer and A. B. Metzner, AIChE J. **15**, 426 (1969).
[27] J. Kim and F. Hussain, Phys. Fluids **5**, 695 (1993).
[28] W. G. Tiederman, T. S. Luchik, and D. G. Boggard, J. Fluid Mech. **156**, 419 (1985).
[29] E. De Angelis, C. M. Caciola, V. S. L'vov, A. Pomyalov, I. Procaccia, and V. Tiberkevich, Phys. Rev. E **70**, 055301 (2004).
[30] V. S. L'vov, A. Pomyalov, I. Procaccia, and V. Tiberkevich, Phys. Rev. Lett. **92**, 244503 (2004).
[31] R. Benzi, E. De Angelis, V. S. L'vov, and I. Procaccia, Phys. Rev. Lett. **95**, 194502 (2005).
[32] T. Min, J. Yoo, H. Choi, and D. D. Joseph, J. Fluid Mech. **486**, 213 (2003).